PCCP

PAPER

View Article Online
View Journal | View Issue

Cite this: *Phys. Chem. Chem. Phys.*, 2017, **19**, 11354

Excitation dynamics involving homogeneous multistate interactions: one and two color VMI and REMPI of HBr†

Helgi Rafn Hróðmarsson,[a] Andreas Kartakoullis,[b] Dimitris Zaouris,‡[b] Pavle Glodic,[b] Huasheng Wang,[a] Peter C. Samartzis *[b] and Ágúst Kvaran *[a]

Received 16th January 2017,
Accepted 3rd April 2017

DOI: 10.1039/c7cp00345e

rsc.li/pccp

Velocity map imaging (VMI) data and mass resolved REMPI spectra are complementarily utilized to elucidate the involvement of homogeneous multistate interactions in excited state dynamics of HBr. The $H^1\Sigma^+(v' = 0)$ and $E^1\Sigma^+(v' = 1)$ Rydberg states and the $V^1\Sigma^+(v' = m + 7)$ and $V^1\Sigma^+(v' = m + 8)$ ion-pair states are explored as a function of rotational quantum number in the two-photon excitation region of 79 100–80 700 cm^{-1}. H^+ and Br^+ images were recorded by one- as well as two-color excitation schemes. Kinetic energy release (KER) spectra and angular distributions were extracted from the data. Strong-to-medium interactions between the E(1) and V(m + 8)/V(m + 7) states on one hand and the H(0) and V(m + 7)/V(m + 8) states on the other hand were quantified from peak shifts and intensity analysis of REMPI spectra. The effects of those interactions on subsequent photoionization and photolytic pathways of HBr were evaluated in one-color VMI experiments of the H^+ and two-color VMI experiments of the Br^+ photoproducts.

I. Introduction

Since the introduction of Velocity Map Imaging (VMI) by Eppink and Parker,[1,2] the study of photofragmentation dynamics has exploded with the applications of both 2D and 3D imaging methods.[3,4] Such experiments yield a wealth of dynamical information regarding the nature of fragmentations and the anisotropy of photoproduct scattering.

Multiphoton excitations of the hydrogen halides have become a benchmark for studies of high energy Rydberg and valence states and the interactions between them. At high energies, the density of states increases, resulting in complex, perturbed spectra where excitation dynamics involve predissociation, autoionization, and numerous state interactions in addition to direct photolysis channels through repulsive states. The dynamics information reservoir on the hydrogen halides is steadily increasing with extensive work performed on HCl,[5–28] HBr,[15,20,28–33] and HI.[15,34–42] Multiphoton excitation coupled with velocity map imaging have been complimentarily utilized to elucidate photofragmentation pathways in HCl,[43–48] HBr,[44,46,47,49–51] and HI.[38]

For HBr, specifically, studies include examination of low energy repulsive state dynamics,[44,49,52,53] photodissociation through intermediate Rydberg states[46,47,51] and ion-pair states,[47,51] superexcited state reconstructions,[50] and formation of bromine atoms from clusters.[54] Some of the experimental studies have utilized *ab initio* calculations,[30,46,53] which turned out to be useful correcting potential curves,[55,56] as well as resolving properties such as ion distributions,[30] spin–orbit branching ratios,[57] and anisotropy parameters.[58]

Recently, one color VMI coupled with (2 + n) REMPI of HBr were used to investigate the effect of interactions between the $E^1\Sigma^+(v' = 0)$ Rydberg state and the $V^1\Sigma^+(v' = m + i, i = 4, 5)$, ion-pair states on subsequent processes such as photoionization and photofragmentation.[51] The state interactions had previously been studied by mass resolved REMPI, based on spectral perturbations.[28] An energetic scheme was proposed to explain the observed perturbation effects. It was found to be helpful in resolving the fragmentation processes examined in the VMI studies,[51] which demonstrated that the total kinetic energy releases and angular distributions of the fragmentation processes were largely dependent on E and V state quantum level resonance excitation and state mixings. More recently a joined study of one-color mass resolved REMPI and VMI of H^+ of HBr, for resonance excitations to the interacting $6p\pi^3\Sigma^-(0^+; v' = 0)$ Rydberg state and the $V^1\Sigma^+(0^+; v' = m + 17)$ ion-pair state

[a] *Science Institute, University of Iceland, Dunhagi 3, 107 Reykjavík, Iceland. E-mail: agust@hi.is; Fax: +354-552-8911; Tel: +354-525-4800*
[b] *Institute of Electronic Structure and Laser, Foundation for Research and Technology-Hellas, Vassilika Vouton, 71110 Heraklion, Greece. E-mail: sama@iesl.forth.gr; Fax: +30-2810-391305; Tel: +30-2810-391467*

† Electronic supplementary information (ESI) available. See DOI: 10.1039/c7cp00345e

‡ Present address: Department of Physics and Astronomy, University College London, Gowen Street London WC1E, 6BT, UK.

revealed the effect of weaker triplet-to-singlet state interaction on photofragmentation dynamics.

In both VMI studies, the initial excitation involved two-photon transitions from the molecular ground state ($\sigma^2\pi^4$) *via* "virtual states" which can borrow character from the repulsive valence states ($\sigma^2\pi^3\sigma^*$), $a^3\Pi_{1,0^+}$, $A^1\Pi_1$ and ($\sigma\pi^4\sigma^*$) $t^3\Sigma^+_{1,0^-}$ accessed by the first photon.[30,44,49,52,54,60] The $a^3\Pi_1$ and $A^1\Pi_1$ repulsive states correlate with H + Br($^2P_{3/2}$), whereas the $a^3\Pi_{0^+}$, and $t^3\Sigma^+_{0^-,1}$ states correlate with H + Br*($^2P_{1/2}$). For simplicity we will hereafter use Br to denote Br($^2P_{3/2}$) and Br* to denote Br($^2P_{3/2}$). Therefore, the one-photon channels are:[59–61]

$$HBr(X^1\Sigma^+\ v' = 0, J') + h\nu \rightarrow HBr(a^3\Pi_1/A^1\Pi_1) \rightarrow H + Br \quad (1a)$$

$$HBr(X^1\Sigma^+\ v' = 0, J') + h\nu \rightarrow HBr(a^3\Pi_{0^+}/t^3\Sigma^+_{0^-,1}) \rightarrow H + Br^* \quad (1b)$$

The two-photon resonance excitations can either involve transitions to Rydberg states, $(\sigma^2\pi^3)nl\lambda$, or ion-pair vibrational states ($\sigma\pi^4\sigma^*$) or corresponding mixed states (commonly denoted here as HBr**),

$$HBr(X^1\Sigma^+\ v' = 0, J') + 2h\nu \rightarrow HBr^{**} \quad \text{two-photon resonance excitation} \quad (2)$$

The absorption of the third photon can involve excitations to singlet and/or triplet repulsive superexcited Rydberg states ($HBr^{\#}$; $^{1,3}\Sigma$, $^{1,3}\Pi$) which correlate with H*(n = 2) + Br/Br*. Excitation to those states is followed either by dissociation or autoionization to form vibrationally excited HBr^+ or HBr^{+*} ions ($\sigma^2\pi^3$):[62,63]

$$HBr^{**} + h\nu \rightarrow HBr^{\#}(^{1,3}\Sigma, {}^{1,3}\Pi) \quad \text{photoexcitation} \quad (3)$$

$$HBr^{\#}(^{1,3}\Pi) \rightarrow H^*(n = 2) + Br \quad \text{dissociation} \quad (4a)$$

$$HBr^{\#}(^{1,3}\Sigma) \rightarrow H^*(n = 2) + Br/Br^* \quad \text{dissociation} \quad (4b)$$

$$HBr^{\#}(^{1,3}\Sigma, {}^{1,3}\Pi) \rightarrow HBr^+(^2\Pi_{3/2}; v^+)/HBr^{+*}(^2\Pi_{1/2}; v^+) + e^- \quad \text{autoionization} \quad (4c)$$

The contributions of the various processes (4) are found to be largely dependent of the nature and mixing of the HBr** state which govern the strength of the photoexcitation process (3) and its dependence on the internuclear distance.

Finally, absorption of a fourth photon produces the detectable ionized fragments. Thus, the vibrationally excited HBr^+/HBr^{+*} ions are excited to repulsive states which correlate with H^+ + Br/Br* while the H* fragments, produced in (4a) and (4b) are ionized

$$HBr^+(v^+)/HBr^{+*}(v^+) + h\nu \rightarrow H^+ + Br/Br^* \quad \text{photodissociation} \quad (5a)$$

$$H^*(n = 2) + Br/Br^* + h\nu \rightarrow H^+ + Br/Br^* + e^- \quad \text{photoionization} \quad (5b)$$

The neutral Br/Br* fragments produced by the processes above can be detected by (2 + 1) REMPI:

$$Br/Br^* + 2h\nu \rightarrow Br^{**} \quad \text{resonance excitation} \quad (6a)$$

$$Br^{**} + h\nu \rightarrow Br^+ + e^- \quad \text{ionization} \quad (6b)$$

The results mentioned above[51,64] became an impetus to study the effects of high energy multistate interactions of varying strength on photofragmentation processes, on a quantum energy level basis. Such studies provide valuable information on how state interactions affect competition between photolytic and ionization pathways in highly excited molecules. In this paper we present data relevant to the effect of singlet-to-singlet state interactions between two Rydberg and two valence states on vibrational and rotational energy level basis. The $E^1\Sigma^+(v' = 1)$ ($(\sigma^2\pi^3)6p\pi$) and $H^1\Sigma^+(v' = 0)$ ($(\sigma^2\pi^3)5d\pi$) Rydberg states and the $V^1\Sigma^+(v' = m + 7)$ and $V^1\Sigma^+(v' = m + 8)$ ion-pair (valence) states ($(\sigma\pi^4)\sigma^*$) of HBr, which are known to exhibit homogeneous Rydberg-to-valence states interactions,[33] were studied by mass resolved REMPI and one- as well as two-color VMI of the H^+ and Br^+ ions, respectively. J'-dependent state mixing as well as state-to-state interaction strengths were extracted from the REMPI spectra for the states involved. Anisotropy parameters relevant to the initial resonance excitation step for the $H^1\Sigma^+(v' = 0)$ state were estimated from line intensities. Kinetic energy release (KER) and angular distributions derived from one-color velocity map images of the ions allowed characterization of the H^+ generation pathways following the interaction. The two-color experiments for Br^+ detection, in particular, proved to be very useful to shed light on the nature of the initial two-photon resonance excitation step. In what follows, the resonance excited states listed above, will be nicknamed E1, H0, V7 and V8 respectively.

II. Experimental

The VMI setup used in this work has been described in detail before.[65,66] Hence, only a brief description will be given here.

A supersonic molecular beam, typically of a mixture of 15% HBr in He, was formed by expansion through a home-made piezoelectrically actuated nozzle valve ($\varnothing$ 1 mm orifice) before being skimmed ($\varnothing$ 1.5 mm, Beam Dynamics) prior to entering the detection chamber of the VMI setup. A stagnation pressure of $P_0 \leq 1$ bar was used.

A photolysis/photofragment ionization laser beam is focused (f = 30 cm) on the geometric focal point of a single-electrode repeller–extractor plate arrangement where it intersects the collimated molecular beam at right angles. In one-color experiments, the laser beam (typically 1.5 mJ per pulse) is generated by a pulsed Nd^{3+}:YAG (Spectra Physics Quanta Ray Pro 250) pumping a master oscillator – power oscillator system (Spectra Physics MOPO 730-10) set at the appropriate wavelength. In two-color experiments, a second excimer-pumped (Lambda Physik LPX300, operating with XeCl) pulsed-dye laser's (Lambda Physik LDP3000) pulses are used with an appropriate dye and a BBO crystal (output typically around 1 mJ per pulse) to ionize quantum-state-selectively (*i.e.* by REMPI) photofragments generated by the MOPO system. In this case, the two lasers are counter-propagating and focused onto the collimated molecular beam by f = 30 cm lenses. To detect Br and Br* fragments (see below), 260.622 nm and 262.540 nm laser pulses were used for the probe (ionization) laser system to achieve (2 + 1) REMPI

through the $4s^2 4p^4(^3P_2)5d(^4D^\circ_{3/2})$ and $4s^2 4p^4(^3P_0)5p(^2P^\circ_{1/2})$ intermediate Rydberg states, respectively.

The probe laser pulses were delayed with respect to the photolysis pulse, in order to allow a sufficient density of photofragments to build up prior to REMPI detection. Moreover, the time delay had to be carefully adjusted in order to avoid "fly-out" of the photofragments. Typically, the delay was set at about 10 ns.

Kinetic energy and angular distributions of photofragments were extracted from images following inverse Abel transforms, (see ref. 67 and references therein) which provided 2D-cuts for the 3D projections of the distributions.

III. Results

A. Mass resolved (2 + *n*) REMPI

Mass resolved (2 + *n*) REMPI spectra of HBr in the two-photon excitation region 79 100–80 700 cm^{-1} have been reported in ref. 33. Therein, the REMPI spectra of the resonance Rydberg states E1 and H0 and the ion-pair states V7 and V8 are presented. An energy diagram of these states, derived from the spectra, is presented in Fig. 1. Perturbation effects in the spectra appear as deviations from linearity in plots of energy level spacing $\Delta E_{J',J'-1}$ $(= E(J') - E(J'-1))$ as a function of J' (Line-shift (LS) effects)[41,42] and as anomalies in ion signal intensity ratio $(I(Br^+)/I(HBr^+))$ as a function of J' (Line intensity (LI) effect). These effects have been interpreted qualitatively as being due to non-degenerate interactions between the Rydberg states and the ion-pair states (*e.g.* see ref. 24, 33 and 41). The observations qualitatively agree with a model of energy level mixings of the same J' quantum numbers, for interacting states. Thus the interactions are manifested as "repulsions of the energy levels" inversely proportional to the energy differences. In ref. 33, weak, near-degenerate interactions between the V7 state and the $F^1\Delta_2(v'=0)$ Rydberg state for $J'=5$–6 was identified and quantified.[33] Now we will use the REMPI data reported in ref. 33 to further quantify interactions between the E1, H0, V7 and V8 states.

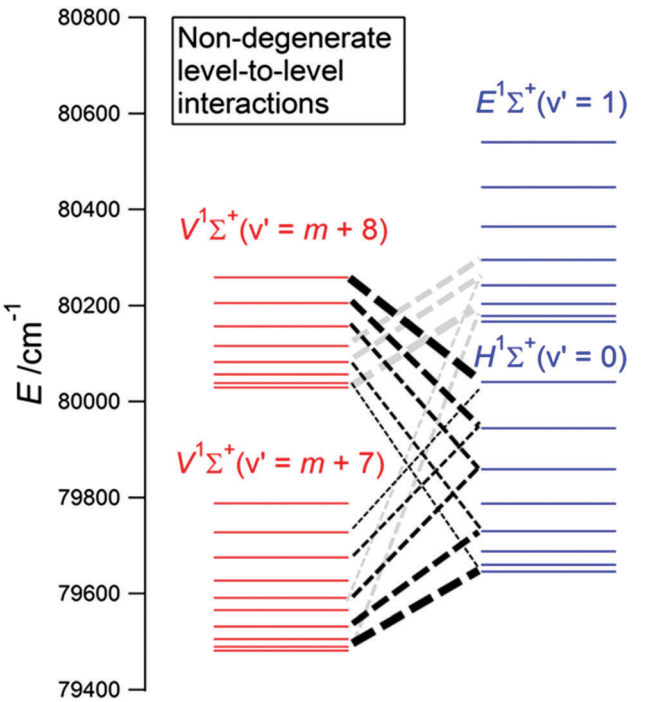

Fig. 1 Rotational energy levels derived from observed (2 + *n*) REMPI spectral lines for the $E^1\Sigma^+(v'=1)$ and $H^1\Sigma^+(v'=0)$ Rydberg (blue) and the $V^1\Sigma^+(v'=m+8)$ and $V^1\Sigma^+(v'=m+7)$ ion-pair (red) resonance excited states. Level-to-level non-degenerate interactions between the Rydberg and ion-pair states are indicated by broken lines. Alterations in state mixing are shown, roughly, by varying thickness of the broken lines.

The shared symmetry $(^1\Sigma^+)$ of the E1, H0, V7, and V8 states means that they will exhibit relatively strong non-degenerate interactions.[28,41,51] By assuming minimum interactions between the Rydberg states, on one hand, and between the ion-pair states, on the other hand, the Hamiltonian matrix simplifies to,

*Xi**Xj*	V7	H0	V8	E1
V7	E^0_{V7}	$W_{H0,V7}$	0	$W_{E1,V7}$
H0	$W_{H0,V7}$	E^0_{H0}	$W_{H0,V8}$	0
V8	0	$W_{H0,V8}$	E^0_{V8}	$W_{E1,V8}$
E1	$W_{E1,V7}$	0	$W_{E1,V8}$	E^0_{E1}

where E^0_{Xi} are the deperturbed energies of the excited states (X), given by

$$E^0_{Xi}(J') = \nu^0 + B'J'(J'+1) \quad (7)$$

as a function of the J' quantum numbers, where the parameters ν^0 and B' represent the band origins and the rotational constants, respectively. The non-zero off-diagonal matrix elements $(W_{Xi,Xj};\ i \neq j)$ represent the interaction strengths between the Rydberg and ion-pair states and are independent of J', since the interactions are homogeneous $(\Delta\Omega = 0)$.[28]

For level-to-level interactions between a Rydberg state (*Xi* = Ry) and one ion-pair state (*Xj* = V) the following expression holds[40] for the fractional state mixing (c_{Ry}^2 and c_V^2).

$$c_{Ry}^2 = \frac{1}{2} + \frac{\sqrt{\left(\Delta E_{Ry,V}(J')\right)^2 - 4\left(W_{Ry,V}\right)^2}}{2\left|\Delta E_{Ry,V}(J')\right|};\ c_V^2 = 1 - c_{Ry}^2 \quad (8)$$

where $\Delta E_{Ry,V}(J')$ is the energy difference between levels of same J' values for the two states. This expression indicates that Rydberg state, Ry, exhibits 100% Rydberg character $(c_{Ry}^2 = 1)$ when $W_{Ry,V} = 0$ (which amounts to 0% ion-pair character), and 50% Rydberg character and 50% ion-pair character $(c_{Ry}^2 = c_V^2 = 0.5)$ when $\Delta E_{Ry,V}(J') = 2W_{Ry,V}$. A corresponding approximation expression can be derived for interactions between a Rydberg state, Ry and two ion-pair states (V*i* and V*j*) by applying two interaction terms and an appropriate normalization,

$$c_{Ry}^2 = \frac{1}{3} + \frac{\sqrt{\left(\Delta E_{Ry,Vi}(J')\right)^2 - 4\left(W_{Ry,Vi}\right)^2}}{3\left|\Delta E_{Ry,Vi}(J')\right|} + \frac{\sqrt{\left(\Delta E_{Ry,Vj}(J')\right)^2 - 4\left(W_{Ry,Vj}\right)^2}}{3\left|\Delta E_{Ry,Vj}(J')\right|};\quad c_V^2 = 1 - c_{Ry}^2 \quad (9)$$

where c_V^2 represents the combined fractional contribution of both ion-pair states (Vi and Vj) (*i.e.* the total ion-pair character in the mixed state). c_V^2 can be further fragmented into the ion-pair contributions of each individual ion-pair state as:

$$c_{Vi}^2 = \frac{1}{3} - \frac{\sqrt{\left(\Delta E_{Ry,Vi}(J')\right)^2 - 4\left(W_{Ry,Vi}\right)^2}}{3\left|E_{Ry,Vi}(J')\right|} \qquad (10)$$

where i = 7 and 8. The maximum individual ion-pair fraction $\left(c_{Vi}^2 = \frac{1}{3}\right)$ is obtained when $2W_{Ry,Vi} = \Delta E_{Ry,Vi}(J')$, and the minimum ($c_{Vi}^2 = 0$), when $W_{Ry,Vi} = 0$. The total as well as the fractional ion-pair contributions (V7 and V8) to the E1 and H0 Rydberg states mixing, as a function of J' are presented in Fig. 2a and b, respectively. W values from Table 1, derived as described in the next paragraphs, were used. For the H0 state, the overall mixing decreases up to J' = 5 and increases for J' = 6, 7. This is the effect of two components: a decreasing contribution of the V7 state and an increasing contribution of the V8 state, which is onset between J' = 4 and J' = 5 (Fig. 2a). For the E state, fractional mixing decreases with J'. The contribution of V8 state decreases with J', whereas the V7 state contribution is almost stable and slightly decreases

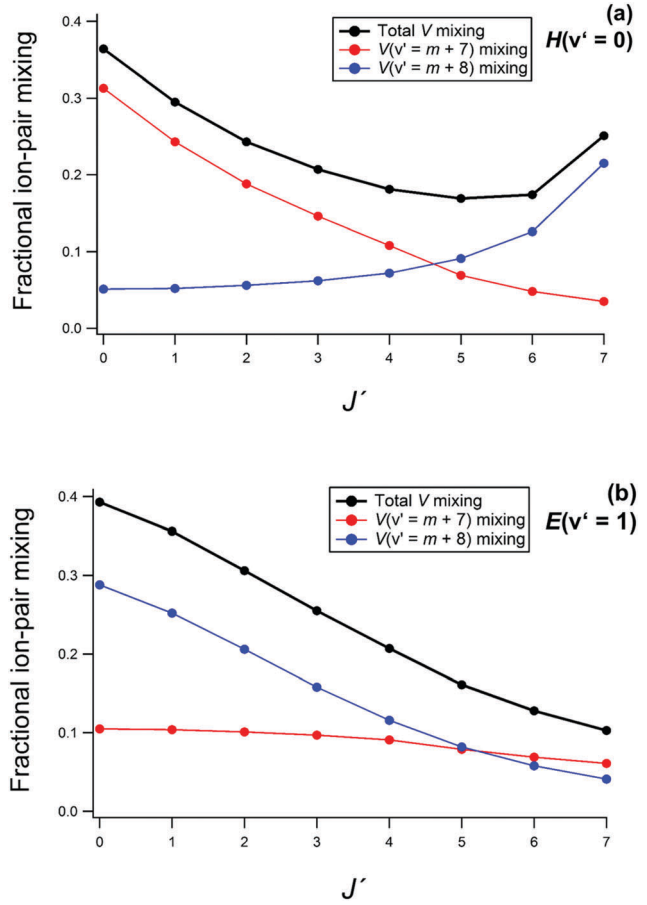

Fig. 2 Total (black) and fractional (blue and red) mixing of the $H^1\Sigma^+(v' = 0)$ (a) and $E^1\Sigma^+(v' = 1)$ (b) Rydberg states with the $V^1\Sigma^+(v' = m + 8)$ and $V^1\Sigma^+(v' = m + 7)$ ion-pair states as a function of J'.

Table 1 Interaction strengths ($W_{Ry,V}$) and rate parameters (α,γ)[26] for the $E^1\Sigma^+(v' = 1)$ and $H^1\Sigma^+(v' = 0)$ Rydberg states (Ry) mixed with the $V^1\Sigma^+(v' = m + 7)$, and $V^1\Sigma^+(v' = m + 8)$ ion-pair states, derived from signal intensity ratios (see main text and eqn (9)–(11))

	$H^1\Sigma^+(v' = 0)$	$E^1\Sigma^+(v' = 1)$
$W_{Ry,V(v'=m+7)}/cm^{-1}$	82	250
$W_{Ry,V(v'=m+8)}/cm^{-1}$	102	68
α	0.7	3
γ	0.4	0.4

above J' = 5 (Fig. 2b). It is noteworthy that the V8 contribution decreases with J' for E1 and increases for H0, whereas the V7 contribution decreases for H0 but remains steady for most low J's in the case of the E1 state.

Approximate values for the interaction strengths, $W_{Ry,Vi}$, were derived by substituting eqn (9), above, into an expression for the intensity ratios $I[Br^+]/I[HBr^+]$ as originally derived by Kvaran *et al.*[26]

$$\frac{I[Br^+]}{I[HBr^+]} = \alpha\frac{\left(\gamma + c_V^2(1-\gamma)\right)}{\left(1 - c_V^2\right)} \qquad (11)$$

where α is a measure of the relative rate of the main formation channel of Br^+ from the ion-pair state (α_V) to the main formation channel of HBr^+ from the Rydberg state (α_{Ry}) (*i.e.* $\alpha = \alpha_V/\alpha_{Ry}$) and γ measures the relative rate of formation of Br^+ from the diabatic Rydberg state (β_{Ry}) to that of its formation from the diabatic ion-pair state (α_V) (*i.e.* $\gamma = \beta_{Ry}/\alpha_V$). The derived values are shown in Table 1. Based on the interaction strengths, the E1–V7 interaction is about three times stronger than the H0–V7 interaction and the H0–V8 interaction is about 50% stronger than the E1–V8 interaction. This suggests that the E1 state interacts mainly with the V7 state and H0 mainly with the V8 state. The values for the interaction strengths were further used to perform simultaneous three-state deperturbation analyses for the two Rydberg states, E1 and H0 interacting with the two ion-pair states, V7 and V8. Derived spectroscopic constants are presented in Table 2, along with parameters derived from standard fittings of the perturbed spectral data.

Comparison of the deperturbed energies ($E^0_{Xi}(J')$), according to eqn (7), and the corresponding perturbed energies ($E_{Xi}(J)$) in the form of the difference values ($E_{Xi}(J') - E^0_{Xi}(J')$) as a function of J' for the four resonance states of concern is presented in Fig. 3.

Positive difference values of about 90–100 cm^{-1} for the E1 state is indicative of an accumulative upwards repulsion of the levels due to the interactions with the V8 and V7 states, whereas negative J'-dependent values for the V7 (−40 to −100 cm^{-1}) state is indicative of an accumulative downwards repulsion due to the interactions with the H0 and E1 states. The dip in the plot for the V7 state near J' = 5–6 is indicative of a near-degenerate interaction with the $F^1\Delta_2(0)$ state, which has been discussed in detail previously.[33] The difference values for the V8 state switch from negative values for low J' (up to J' = 4) to positive values for higher J' (−30 to +50 cm^{-1}) as a result of the

Table 2 Band origins (ν^0) and rotational constants ($B_{\nu'}$, $D_{\nu'}$) derived from perturbed mass resolved REMPI spectra ("Measured"), deperturbation analysis ("Deperturbed") of the spectra along with values derived by others from measured spectra

State	ν^0/cm^{-1} Deperturbed/measured/others[29]	$B_{\nu'}$/cm^{-1} Deperturbed/measured/others[29]	$D_{\nu'}$/cm^{-1} Deperturbed/measured/others[29]
$V^1\Sigma^+(v' = m + 7)$	79 584 ± 11/79481.3/79480.3	2.7 ± 0.2/3.6/—	—/0.000/—
$H^1\Sigma^+(v' = 0)$	79 817 ± 31/79645.6/79645.5	7.7 ± 0.5/7.1/7.193	—/0.010/0.0006
$V^1\Sigma^+(v' = m + 8)$	80 056 ± 35/80029.0/80029.7	2.8 ± 0.6/4.4/—	—/0.0027/—
$E^1\Sigma^+(v' = 1)$	80 076 ± 4/80166.3/80168.8	6.3 ± 0.5/6.4/5.93	—/−0.008/−0.028

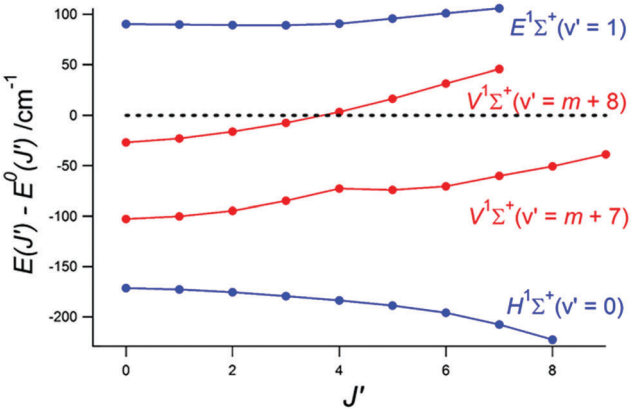

Fig. 3 Reduced term value (RTV) plots for the $E^1\Sigma^+(v' = 1)$ and $H^1\Sigma^+(v' = 0)$ Rydberg states (blue) and the $V^1\Sigma^+(v' = m + 8)$ and $V^1\Sigma^+(v' = m + 7)$ ion-pair states (red).

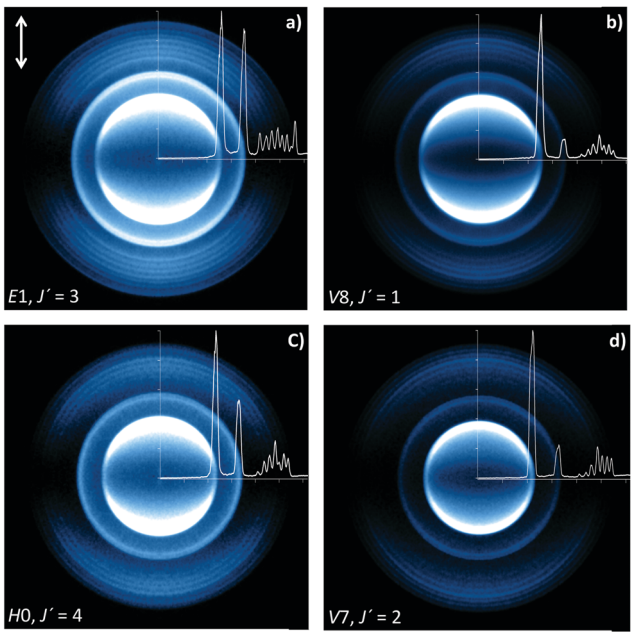

Fig. 4 One color H^+ velocity map images and corresponding kinetic energy release (KER) spectra for two-photon resonance excitations to the (a) E($v' = 1$); $J' = 3$, (b) V($v' = m + 8$); $J' = 1$, (c) H($v' = 0$); $J' = 4$ and (d) V($v' = m + 7$); $J' = 2$ resonance energy levels *via* the Q branch. The image intensity scale has been adjusted for the outer rings to be visible. The KER spectra are normalized to the peak of the innermost ring (Br* channel; see main text). The laser polarization is indicated by the double arrow in panel (a).

accumulative upwards and downwards J'-dependent repulsions due to the interactions with the H0 and E1 states, respectively. A large downward repulsion of the H0 state levels (−220 to −170 cm^{-1}), which is due to the accumulative upwards and downwards J'-dependent repulsions due to the interactions with the V7 and V8 states, respectively, is indicative of the larger interaction effect of the V8 state rather than the V7 state (see Table 1).

B. One color VMI

H^+ images and kinetic energy release (KER) spectra. H^+ images were recorded for one-color, two-photon resonance excitations from the ground state X0(J'') to the H0($J' = 0$–9) and E1($J' = 0$–6) Rydberg states, and the V7($J' = 1$–8) and V8($J' = 0$–7) ion-pair states of HBr for the Q rotational lines ($J' = J''$). In all of the images, two intense rings are observed at low and medium KERs and a group of weaker ones for high KERs (see Fig. 4). These images resemble those previously reported for various Rydberg and ion-pair states of HBr.[50,51,64] The two intense inner rings correspond to photofragmentation of superexcited states towards H*($n = 2$) + Br/Br* (see mechanisms 4a and 4b in Section I) and subsequent photoionization of H*($n = 2$) (process 5b in Section I). The innermost ring corresponds to the formation of Br* + H*($n = 2$) (named Br* channel hereafter) whereas the ring of medium KER corresponds to the formation of Br + H*($n = 2$) (Br channel hereafter). The weaker outermost rings correspond to H^+ formed by autoionization of superexcited HBr (channel 4c in Section I) followed by photodissociation of the molecular ion in various vibrational levels (v^+) (channel 5a in Section I) (HBr^+ channel). Fig. 5 shows the KER spectrum for the H0($J' = 0$) resonance state, as an example. The two KER peaks at ∼0.4 and ∼0.8 eV correspond to the two intense inner rings in Fig. 4, whereas the group of high energy peaks between 1.3 and 2.5 eV correspond to the outermost rings.

The relative signal strengths (I_{rel}) of the various channels, defined as the integrated signal intensities, I(i), of the channels (i) divided by the total integrated intensities (ΣI(i)) (*i.e.* $I_{rel} = I(i)/\Sigma I(i)$) are shown in Fig. 6 as a function of J' for the various resonance states. For the V8, H0 and V7 states the I_{rel} values vary, overall, as channel Br* > channel HBr^+ > channel Br, whereas, for E1 all the I_{rel} are comparable. There is a clear distinction between the J' dependences of I_{rel} for the Br channel on one hand and the Br* and HBr^+ channels on the other hand. The I_{rel} for the Br channel varies only slightly with J' in all states. The I_{rel}

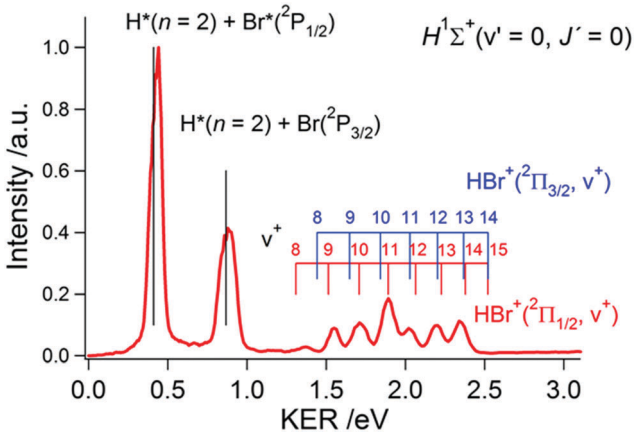

Fig. 5 H^+ kinetic energy release (KER) spectrum for resonance excitation from the ground state, X(v'' = 0, J'' = 0) to the H(v' = 0, J' = 0) state. Peaks corresponding to H^+ formation *via* the Br* (~0.4 eV) and Br (~0.8 eV) channels (see main text) are marked. Predicted peak positions (assignments of peaks), with respect to the intermediate vibrational levels of the HBr^+/HBr^{*+} ionic states (v^+) (1.3–2.5 eV) for the HBr^+ channels are also shown.

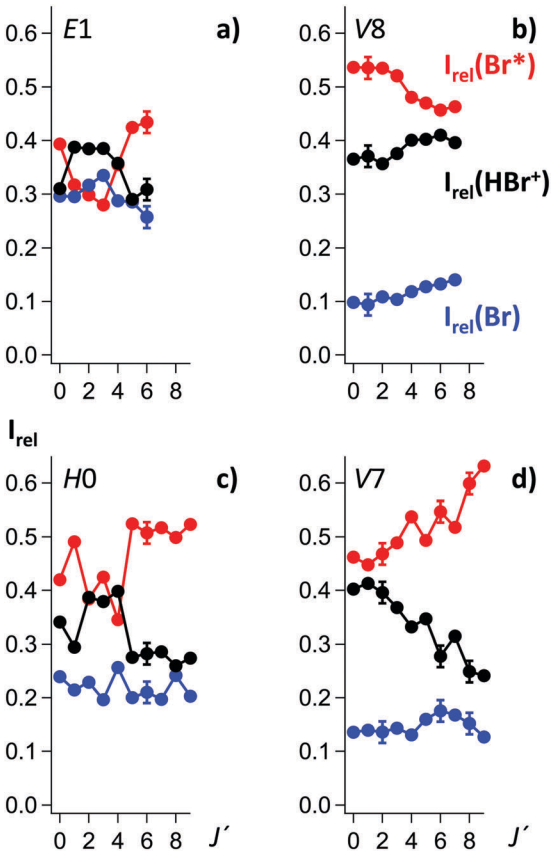

Fig. 6 Branching ratios: relative integrated H^+ signal intensities (I_{rel}; see main text) of the various H^+ formation channels (Br* (red), Br (blue) and HBr^+ (black)) as a function of J' (for $J'' = J'$; Q lines) for the resonance excited states E(v' = 1) (a), V(v' = m + 8) (b), H(v' = 0) (c) and V(v' = m + 7) (d).

plots for the Br* and HBr^+ channels show more significant variations with J' as well as "near-mirror image effects" such that increases in values for one of those channels correspond to decreases in the other and *vice versa*. These effects will be discussed further in Section IV.

Angular distributions of H^+. Most of the rings display shapes corresponding to overall parallel transitions (Fig. 4). Only the rings, corresponding to the Br channel, for V8, J' = 6 and H0, J' = 4–5 display structure of overall perpendicular transitions.

In an attempt to quantify the anisotropy of the rings/channels, the angular distributions were fitted by a simplified expression corresponding to a one-step photodissociation,[51]

$$P(\theta) = A(1 + \beta_2 P_2(\cos(\theta)) + \beta_4 P_4(\cos(\theta))) \quad (12)$$

where β_2 and β_4 are the corresponding anisotropy parameters and A is a scaling factor. The beta parameters, being "effective" parameters for the overall photodissociation/photoionization processes that lead to H^+ formation, can then be related to the overall transition symmetry and the corresponding dynamics. In most cases insignificant variations in the parameter β_2/angular distributions were observed with J'. Therefore, we present only averaged values of the β_2 parameter for the various H^+ formation channels in Table 3. One J'-dependent observation is a significant lowering in β_2, hence increasing perpendicular character of the corresponding transition, observed for the Br channel of the V8 ion-pair resonance state, with increasing J' for J' = 0–6.[68] A second J'-dependent observation occurs in the H0 state, where a minimum value of the β_2 parameter (hence, largest perpendicular transition character) is obtained for J' = 4–5 (see Fig. 7a and ref. 68). For the E1, V8 and H0 states the β_2 parameters vary, mostly, as channels HBr^+ > channels Br* > channels Br, whereas for the V7 state, channels Br > channels HBr^+ > channels Br* (see Table 3 and ref. 68).

The mass resolved REMPI spectra of the H0 resonance state showed clearly resolved O and S rotational lines, which allowed a "two-step analysis" of the angular distributions, corresponding to a one-step resonance excitation followed by a second ionization step.[46,51,63] The angular distributions were expressed by

$$P(\theta) = AP_f(\theta)P_{ph}(\theta) \quad (13)$$

for

$$P_f(\theta) = 1 + \beta_{f,2}P_2(\cos(\theta)) + \beta_{f,4}P_4(\cos(\theta)) \quad (14a)$$

$$P_{ph}(\theta) = 1 + \beta_{ph,2}P_2(\cos(\theta)) + \beta_{ph,4}P_4(\cos(\theta)) \quad (14b)$$

Table 3 Averaged (over J') β_2 values for the $V^1\Sigma^+(v' = m + 7)$ and $V^1\Sigma^+(v' = m + 8)$ ion-pair and the $E^1\Sigma^+(v' = 1)$ and $H^1\Sigma^+(v' = 0)$ Rydberg resonance states derived from the angular distributions of the H^+ images for the major formation channels (see main text), by assuming a one-step photodissociation[51]

	Average values of β_2		
State	Br channels	Br* channels	HBr^+ channels
V7	1.6 ± 0.1	0.6 ± 0.1	1.3 ± 0.1
H0	0.3 ± 0.4	1.1 ± 0.1	1.7 ± 0.2
V8	0.4 ± 0.5	1.2 ± 0.3	1.4 ± 0.1
E1	0.6 ± 0.1	1.3 ± 0.2	1.6 ± 0.1

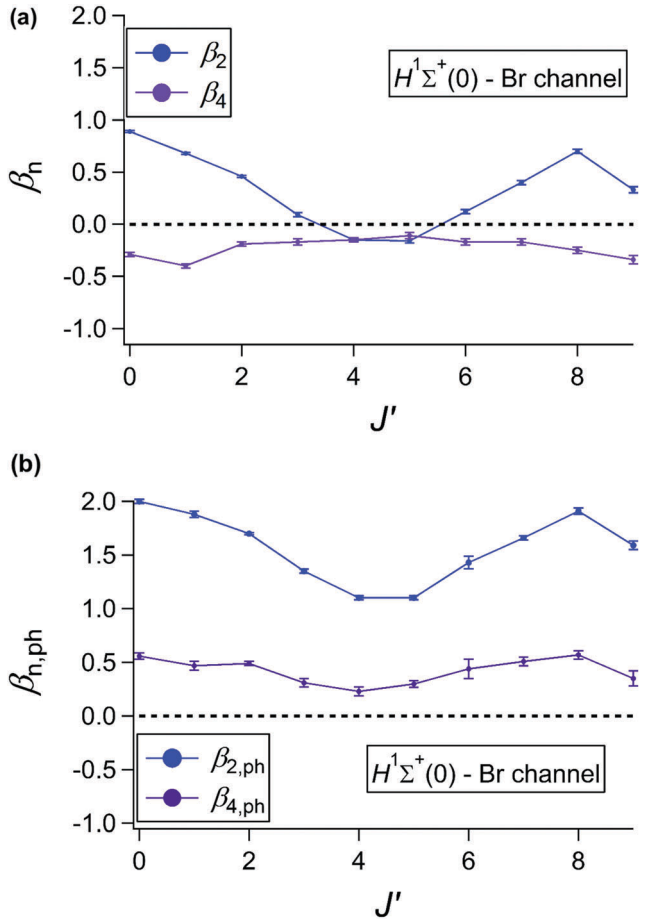

Fig. 7 Anisotropy parameters for the H^+ formation *via* the H* + Br channels for the resonance excitations to the $H^1\Sigma^+(0)$ Rydberg state as a function of J' for $J'' = J'$ (Q lines). (a) Anisotropy parameters, β_2 (blue) and β_4 (violet) obtained from "one-step analysis" (see main text). (b) Anisotropy parameters, $\beta_{2,ph}$ (blue) and $\beta_{4,ph}$ (violet), obtained from "two-step analysis" (see main text).

where $P_f(\theta)$ and $P_{ph}(\theta)$ represent the distributions of the resonance excitation and photofragmentation steps, respectively. The anisotropy parameter of the resonance step, $\beta_{f,2}$, were estimated from[51,63]

$$\beta_{f,2} = \frac{2 - 20\mathrm{Re}[b]}{2 + 25|b|^2} \quad (15)$$

where the b parameter was extracted from the intensity ratios of the Q, S, and O rotational lines based on,

$$\frac{I_Q}{I_S} = \frac{10}{3}\frac{(2J''+1)}{(J''+2)}\left[|b|^2\frac{(2J''+3)}{(J''+1)} + \frac{1}{5}\frac{J''}{(2J''-1)}\right] \quad (16a)$$

$$\frac{I_Q}{I_O} = \frac{10}{3}\frac{(2J''+1)}{(J''-1)}\left[|b|^2\frac{(2J''-1)}{J''} + \frac{1}{5}\frac{(J''+1)}{(2J''+3)}\right] \quad (16b)$$

Thus, $\beta_{f,2}$= −0.92 was obtained which corresponds to a virtually pure perpendicular ($\Sigma \leftarrow \Pi \leftarrow \Sigma$) resonance transition, in close correspondence with our previous two-step analysis for the $E^1\Sigma^+(0)$ resonance state.[52] For a fixed value of $\beta_{f,2}$ = −0.92, the anisotropy parameters, $\beta_{ph,2}$, $\beta_{ph,4}$, and $\beta_{f,4}$, were derived from fittings of the angular distribution by eqn (13). Generally the $\beta_{ph,2}$ and $\beta_{ph,4}$ parameters are found to be larger than the corresponding β_2 and β_4 parameters, derived from the one-step analysis, whereas the J'-dependent variations are found to be virtually unchanged. This is analogous to what has been found for the $E^1\Sigma^+(v' = 0)$ resonance state.[51] Fig. 7b shows the J' dependent parameters for the Br channel. The two-step analysis of the other channels (Br*, HBr^+/HBr^+*), gave $\beta_{ph,2}$ values about +2 for all J's, corresponding to a purely parallel photofragmentation transition. The $\beta_{f,4}$ parameter was found to be about constant ($\sim 0.3 \pm 0.1$) for all the H^+ formation channels. We suggest that the parameters derived by the one-step analysis (β_2 and β_4) can be viewed as lower limit values for the corresponding photofragmentation steps ($\beta_{ph,2}$, $\beta_{ph,4}$).

C. Two color VMI

Br^+ images and kinetic energy release (KER) spectra. Images of Br^+ were recorded for two-photon resonance excitation from the ground state to the H0 and E1 Rydberg states and the V7 and V8 ion-pair states, as a function of J', following (2 + 1) REMPI of $Br(^2P_{3/2})$ and $Br^*(^2P_{1/2})$ (see Section II). Only one major ring was observed for the Br fragment with angular distribution suggesting a perpendicular transition, whereas in Br* images two major rings are present, the inner corresponding to parallel and the outer to perpendicular transition. Kinetic energy release (KER) spectra were derived from the images (Fig. 8). The peaks in the Br spectra appear at approximately 1.0 eV kinetic energy, which correspond to one-photon photodissociations to form H + Br (see process (1a) in Section I). The lower energy KER peak in the Br* spectra appear at $\sim$0.8 eV, which corresponds to one-photon photodissociations to form H + Br* (1b). The higher energy KER peak, which appear at $\sim$5 eV, corresponds to the two-photon molecular

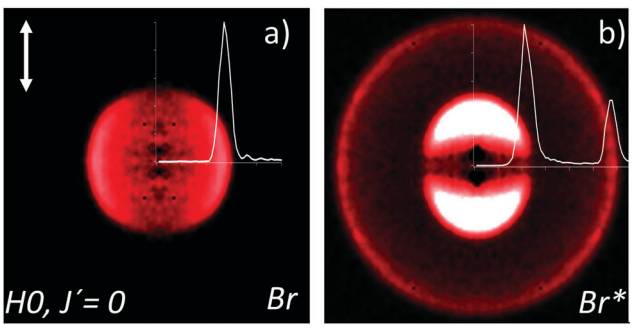

Fig. 8 Two-color Br^+ velocity map images and corresponding kinetic energy release (KER) spectra for two-photon resonance excitations to the H(v' = 0); J'= 0 energy level *via* the Q branch (a) – for (2 + 1) Br REMPI detection and (b) – for (2 + 1) Br* REMPI detection (see Section II).The KER spectra are normalized to the peak of the innermost ring (Br* channel; see main text). The intensity of the image in (b) is adjusted to make the outer ring visible. The laser polarization is indicated by the double arrow in panel (a).

resonance excitation followed by predissociation *via* the repulsive states that yield H + Br*.

Angular distributions of Br^+. One-step analyses (eqn (12)) of the angular distributions (see Fig. 8) gave values for the anisotropy parameter β_2 of about −1 for all the Br rings and about +2 for all the lower energy Br* rings. This corresponds to purely perpendicular and parallel transitions for the two one-photon photodissociation channels (1a) and (1b), respectively. Values for β_2 of about −1, corresponding to virtually purely perpendicular two-photon transitions were derived from the higher energy Br* rings for the E1, V8 and V7 resonance states. For the H0 state an average value of about −0.3 was obtained suggesting dominating perpendicular transitions with some parallel transition contribution. These findings will be further discussed in next Section.

IV. Discussion

A. Mass resolved (2 + *n*) REMPI

The deperturbation analysis of the REMPI spectra coupled with intensity ratio analyses, described in Section III, A, reveal strong to medium interactions between the Rydberg states, E1 and H0 and the ion-pair states V8 and V7 (Table 1) and allow evaluations of spectroscopic parameters for the states (Table 2). The non-degenerate level-to-level nature of the interactions appears as mixing (Fig. 2) and repulsion (Fig. 3) of levels with same J' quantum numbers varying smoothly with J'. The fractional mixing of the E1 state with the ion-pair states is found to decrease with J' (Fig. 2b), which is in agreement with earlier predictions[33] based on signal intensity ratios. Fractional mixing of the H0 state with the ion-pair states is found to be minimal for $J' \sim 5$ (Fig. 2a), which is also in agreement with predictions based on signal intensity ratios.[33] The interactions result in greater divergences of the rotational energies (increasing $E(J') - E^0(J')$) with J' for the ion-pair states but in corresponding compressions (decreasing $E(J') - E^0(J')$ with J') of the levels for the H0 state (Fig. 3), as might be expected.[15]

B. One color VMI

The H^+ formation channels, observed occur *via* one-photon transitions from the mixed resonance excited states (E1, H0, V8 and V7; HBr**) to repulsive superexcited states ($HBr^{\#}$) in the Rydberg series which converge to the ionic states, $B^2\Sigma^+$ $(\sigma^2(\pi_x^1\pi_y^1)\sigma^{*1})$ and $^2\Pi(\sigma^1\pi^3\sigma^{*1})$[47,51,56,64] and which correlate with H*(n = 2) + Br*/Br (Fig. 9a). Considering one-electron transitions and the principal electron configurations, $([\sigma^2\pi^3]5p\pi^1)$ for E1, $([\sigma^2\pi^3]4d\pi^1)$ for H0 and $(\sigma^1\pi^4\sigma^{*1})$ for V8 and V7, the Rydberg electrons must occupy a 5pπ orbital in the case of the E1–V8, V7 mixed states and a $4d\pi^1$ orbital in the case of the H0–V8, V7 mixed states. Although the selection rule for spin conservation favours the involvement of singlet Rydberg states, triplet states cannot be ruled out. Therefore, possible Rydberg states are $^{1,3}\Pi([B^2\Sigma^+;\sigma^2(\pi_x^1\pi_y^1)\sigma^{*1}]Ry\pi^1)$ and $^{1,3}\Sigma([^2\Pi;\sigma^1\pi^3\sigma^{*1}]Ry\pi^1)$ for Ryπ = 5pπ and 4dπ, respectively. Three major transitions for each mixed state systems are, therefore, expected to be involved, two from $([\sigma^2\pi^3]Ry\pi^1)$ (E1/H0; dominating short-range excitations) and one from $(\sigma^1\pi^4\sigma^{*1})$

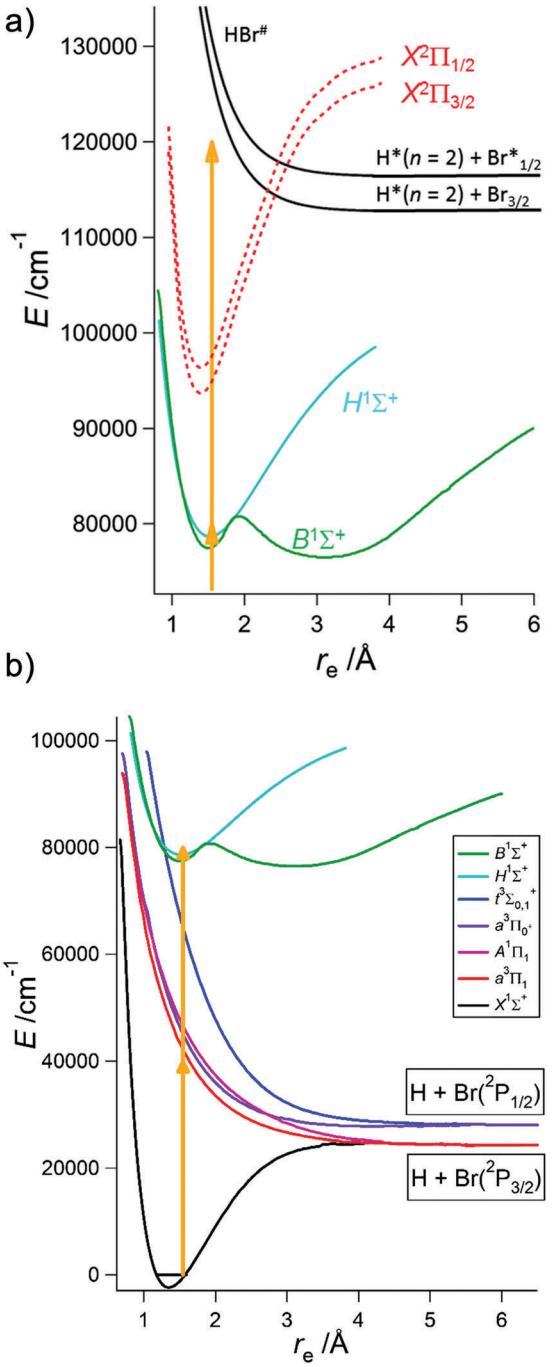

Fig. 9 (a) Potential curves of the states involved in the H^+ formation following two-photon resonance excitation of HBr to the E(v' = 1), H(v' = 0), V(v' = m + 8) and V(v' = m + 7) mixed states, asymptotic energies of fragments and relevant transitions (see main text). The potential curve for the B states (green solid curve) was derived from Fig. 1 in ref. 50. The potential curves for the ionic states (broken curves) were derived from ref. 56. The potential curve of the H state was derived from known origins of the v' = 0, 1, 2 states.[29] The shape of the repulsive states correlating with H* + Br/Br* and H** + Br are based on preliminary *ab initio* calculations,[71] which suggest that the curves might be of shapes close to that of the $B^2\Sigma$ ionic state.[71] (b) Potential curves of the states involved in the two-photon resonance excitation, asymptotic energies of the fragments detected by two-color experiments and relevant transitions (see main text). The relevant potential energy curves were derived from ref. 53.

(V8, V7; longer-range excitation), as (orbital transitions are highlighted, underlined and bold)

(a) $HBr^{**}\{E/H^1\Sigma([^2\Pi;\sigma^2\underline{\boldsymbol{\pi}}^3]Ry\pi^1)\} + h\nu$

$\rightarrow HBr^{\#}\{^{1,3}\Pi([B^2\Sigma^+;\sigma^2(\pi_x^1\pi_y^1)\underline{\boldsymbol{\sigma}}^{*1}]Ry\pi^1)\}$

perpendicular core electron transition/$\underline{\boldsymbol{\pi}} \rightarrow \underline{\boldsymbol{\sigma}}^*$

(b) $HBr^{**}\{E/H^1\Sigma([^2\Pi;\underline{\boldsymbol{\sigma}}^2\pi^3]Ry\pi^1)\} + h\nu$

$\rightarrow HBr^{\#}\{^{1,3}\Sigma([^2\Pi;\sigma^1\pi^3\underline{\boldsymbol{\sigma}}^{*1}]Ry\pi^1)\}$;

parallel core electron transition/$\underline{\boldsymbol{\sigma}} \rightarrow \underline{\boldsymbol{\sigma}}^*$

(c) $HBr^{**}\{V^1\Sigma(\sigma^1\underline{\boldsymbol{\pi}}^4\sigma^{*1})\} + h\nu$

$\rightarrow HBr^{\#}\{^{1,3}\Sigma([^2\Pi;\sigma^1\pi^3\sigma^{*1}]Ry\pi^1)\}$;

parallel core to Rydberg electron transition/$\underline{\boldsymbol{\pi}} \rightarrow \underline{\mathbf{p}\boldsymbol{\pi}}$

The superexcited $HBr^{\#}\{^{1,3}\Sigma([^2\Pi;\sigma^1\pi^3\underline{\sigma}^{*1}]Ry\pi^1)\}$ states will correlate with H* + Br* as well as the H* + Br fragments, corresponding to the two spin–orbit components of the ion cores, whereas the $HBr^{\#}\{^{1,3}\Pi([B^2\Sigma^+;\sigma^2(\pi_x^1\pi_y^1)\underline{\sigma}^{*1}]Ry\pi^1)\}$ states will only correlate with H* + Br. Furthermore, these can autoionize to form HBr^{+}* and $HBr^+(X^2\Pi(\sigma^2\pi^3))$ *via* the Auger effect. We will now consider how the results presented in Section III B match these proposed excitation processes.

The resonance transitions for the mixed H0 state (see Section II B) as well as the $E^1\Sigma^+(v' = 0)$ state[51] are found to be largely perpendicular (*i.e.* $\Sigma \leftarrow \Pi \leftarrow \Sigma$). There is not a reason to expect a large variation in the character of those transitions over the relatively short excitation region of concern here. We, therefore, suggest that the major variations in the overall parallel *vs.* perpendicular transition characters as a function of J', as well as for the different channels (a)–(c) (see above) are associated with the steps following the resonance excitation to HBr**. Therefore, in the cases of the Br* and Br channels, variations in the transition characters will be determined by the relative contributions of the steps (a)–(c) above. In the case of the HBr^+ channels both the steps (a)–(c) and photodissociation of HBr^+/HBr^{+}* need to be considered.

Br channel. Judging from the relative intensities (I_{rel}) of the KER spectra for the various main channels (Fig. 6) the contributions of the Br channels to the overall signal is found to be lower for the ion-pair states (V8 and V7) than for the Rydberg states (E1 and H0). This suggests that the Br signal can be largely associated with short range (short internuclear distance) transitions corresponding to larger Rydberg character of the mixed states. Furthermore, there is a slight enhancement in those signals for the V8 state with J' for J' = 0–6, which correlates with the predicted lowering in the ion-pair character, hence increasing Rydberg character, with J' (Fig. 2a and b). Relatively low β_2 values (0.3–0.6) for the Br channels for all the states except V7 compared to those values for the other channels (1.1–1.7) (Table 3), hence relatively larger perpendicular transition contribution (*i.e.* excitation channel (a) above), further supports this. The dip observed in the plots for β_2 and $\beta_{ph,2}$ *vs.* J' for the Br channels (Fig. 7), hence increased perpendicular transition contribution, for J' = 4–5, correlates well with the predicted minimum of the ion-pair character in the mixed H0 state of $J' \sim 5$ (see Fig. 2a and ref. 33). Furthermore, a decreasing β_2 value with J' for J' = 0–6 of the V8 state (see Section III B and ref. 68) also correlates nicely with the observed increase in I_{rel} with J' for the Br channel (Fig. 6).

The Br* and HBr^+ channels. The close correlation between the I_{rel} *vs.* J' plots for the Br* and HBr^+ channels, that appear as "near-mirror image effects" (Fig. 6), strongly suggests that these channels involve joined transitions from the resonance excited state(s) followed by a competition between the HBr^{+}*/HBr^+ and H* + Br* formations, depending on the degree of the state mixing. This suggests that the Br* and HBr^+ contributions are a reflection of the degree of state mixing. Considering this and the fact that the sum of the relative intensities (see Fig. 6) for those two channels (I_{rel}(Br*) + I_{rel}(HBr^+)) are found to be larger for the ion-pair states (V8 and V7) than for the Rydberg states (E1 and H0) makes us believe that these signals are largely associated with long range transitions corresponding to larger ion-pair states character of the mixed states.

C. Two color VMI

The perpendicular nature of the one-photon transition which results in the Br formation (see Section III C and Fig. 8) is in agreement with observations by others for the excitation energy region of concern (39 700–40 300 cm^{-1}; 248–252 nm).[60,69] It indicates that excitations to the repulsive $a^3\Pi_1$ and $A^1\Pi_1$ valence states (electron configurations $(\sigma^2\pi^3)\sigma^{*70}$) from the $X^1\Sigma^+$ ground state ($\sigma^2\pi^4$) are the major transitions ($\pi \rightarrow \sigma^*$; see eqn (1a) in Section I) involved (see Fig. 9b). The absence of Br peaks (Fig. 8), corresponding to energy release of two-photon absorption to the resonance states indicates that these intermediate states are of minor importance as predissociating states for all the resonance excited states (E1, H0, V8 and V7).

The parallel nature of the one-photon transition which results in Br* formation (see Section III C and Fig. 8) is also in agreement with observations and predictions by others.[53,60,69] It indicates that excitations to the repulsive $t^3\Sigma^+_{1,0^-}$ valence states ($(\sigma\pi^4)\sigma^*$) from the ground state are the major transitions ($\sigma \rightarrow \sigma^*$) involved (see Fig. 9b). The observation of the higher kinetic energy ring, corresponding to two-photon excitations, and its perpendicular transition symmetries, for the Br* detection, for all the states, on the other hand, indicates that two-photon resonance transitions *via* the $a^3\Pi_{10^+}$ and $A^1\Pi_1$ states to give overall perpendicular resonance transitions ($\Sigma \leftarrow \Pi \leftarrow \Sigma$) is a precondition. This requires that the repulsive $t^3\Sigma^+_{1,0^-}$ state/s do not partake as virtual states in the two-photon resonance excitations, in agreement with the calculated $\beta_{f,2}$ parameter for the H0 state ($\beta_{f,2} = -0.92$). A likely predissociation pathway is through interaction between the H0, E1, V7 and V8 mixed states and the $t^3\Sigma^+$ state to give H + Br* (eqn (1b) in Section I). The large average internuclear distance of the V state makes crossing to the repulsive states highly improbable. The Rydberg states, however, are crossed by the repulsive states, thus making predissociation processes more probable.

Hence, the predissociation is likely to occur *via* a dominating Rydberg state character of the mixed states.

V. Conclusions

By joint forces of mass resolved (2 + 1) resonance enhanced multiphoton ionization ((2 + *n*) REMPI) spectra of HBr and velocity map imaging (VMI) of H^+ ions in one-color experiments and of Br^+ ions in two-color experiments the excitation dynamics of the interacting $E^1\Sigma^+(v' = 1)$ (*i.e.* E1) and $H^1\Sigma^+(v' = 0)$ (H0) Rydberg states and the $V^1\Sigma^+(v' = m + 8)$ (V8) and $V^1\Sigma^+(v' = m + 7)$ (V7) ion-pair states has been further clarified.

The aforementioned (2 + *n*) REMPI processes can be viewed as if they are occurring *via* two groups of strongly interacting and J'-dependently mixed resonance states, namely the E1, V8 and V7 states on one hand and the H0, V8 and V7 states on the other hand (Fig. 10). The interaction strengths and the fractional mixings were quantified by analysis of spectral perturbations, which also allowed characterization of the deperturbed states involved.

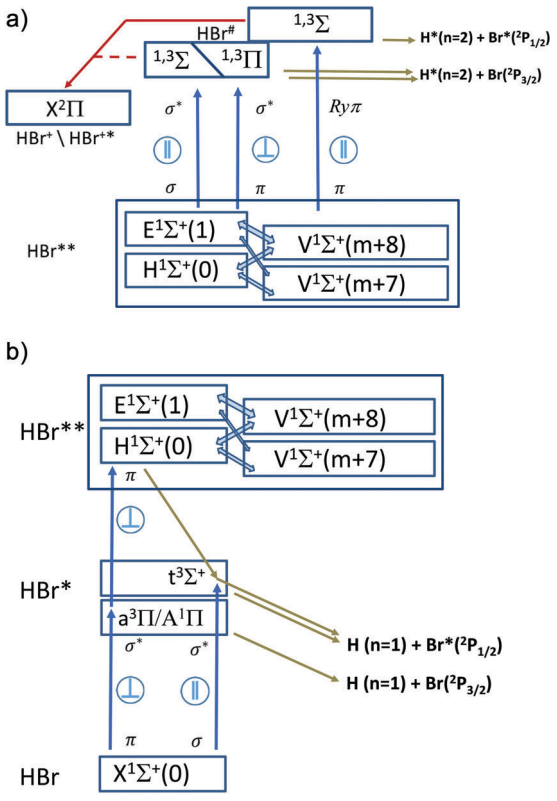

Fig. 10 (a) Schematic figure of the major one-photon transitions (blue arrows) as well as photodissociation (gray arrows) and autoionization (red arrows) processes following two-photon resonance transitions to the E($v' = 1$), H($v' = 0$), V($v' = m + 8$) and V($v' = m + 7$) mixed states, prior to ionization (see main text). Orbital transitions and the nature (parallel/perpendicular transitions) of the photoexcitations are indicated. (b) Schematic figure of the major transitions (blue arrows) involved in the two-photon resonance transitions to the E($v' = 1$), H($v' = 0$), V($v' = m + 8$) and V($v' = m + 7$) mixed states as well as photodissociation and predissociation processes (gray arrows) (see main text). Orbital transitions and the nature (parallel/perpendicular transitions) of the photoexcitations are indicated.

KER spectra and angular distributions of the ions, derived from the one-color H^+ images allowed clarification of the photoionization processes of the mixed resonance states to form the H^+ ions. The processes are believed to involve one-photon transitions to superexcited Rydberg states $HBr^{\#\ 1,3}\Pi$ and $HBr^{\#\ 1,3}\Sigma$, which correlate with $H^*(n = 2) + Br(^2P_{3/2})$ (*i.e.* the $^{1,3}\Pi$ states and the lower spin–orbit components of the $^{1,3}\Sigma$ states) and $H^*(n = 2) + Br^*(^2P_{1/2})$ (the higher spin–orbit components of the $^{1,3}\Sigma$ states) and converge to the ionic states, $B^2\Sigma^+$ and $^2\Pi$, respectively. Excitations to the lower energy superexcited states involve both parallel and perpendicular transitions, largely associated with short range transitions corresponding to dominating Rydberg character in the mixed resonance states, whereas those to the higher energy superexcited states are parallel in nature, largely associated with long range transitions corresponding to dominating ion-pair character in the mixed resonance states. The former transitions will lead to dissociations to form H* + Br, prior to further one-photon ionization of H* to form H^+. The latter transitions can lead to dissociations to form H* + Br*, prior to further one-photon ionization of H* to form H^+ as well as autoionization to form HBr^{+}* and HBr^{+}* prior to photodissociations to form H^+(Fig. 10a).

KER spectra and angular distributions of the ions, derived from the two-color Br^+ images allowed clarification of photoexcitation and photodissociation processes involved in the resonance excitation step. In addition to contributing to the character of virtual states for the two-photon resonance excitations the repulsive valence states, which correlate with the H + Br/Br* fragments, also act as intermediate states for corresponding one-photon photodissociation processes. Thus, H + Br and H + Br* fragments are found to be formed by one-photon excitations to the $a^3\Pi/A^1\Pi$ and $t^3\Sigma^+$ states, respectively. Whereas no or negligible H + Br formation is found to occur by predissociation of the mixed resonance excited state H + Br* is formed by predissociation by the $t^3\Sigma^+$ state at short ranges, corresponding to a dominating Rydberg state character of the mixed states (Fig. 10b).

Acknowledgements

The financial support of the University Research Fund, University of Iceland and the Icelandic Science Foundation (Grant No. 130259-051) is gratefully acknowledged. The research leading to these results has received funding from LASERLAB-EUROPE (grant agreement no. 228334, EC's Seventh Framework Programme). This work was supported by Greek Secretariat for Research and Technology programs ERC03:ITSSUED and THALIS:ISEPUMA, co- financed by EU (European Social Fund) and national funds under NSRF2007–2013. PCS gratefully acknowledges support from an EU Marie Curie Reintegration Grant (GPSDI, Grant No. PIRG07-GA-2010-268305). DZ gratefully acknowledges EU Marie Curie IAPP program SOFORT (GA 251598). We wish to thank Gabriel J. Vázquez, H. P. Liebermann and H. Lefebvre-Brion for useful information concerning HBr potential curves based on unpublished calculations.

References

1 A. Eppink and D. H. Parker, *Rev. Sci. Instrum.*, 1997, **68**, 3477–3484.
2 D. H. Parker and A. Eppink, *J. Chem. Phys.*, 1997, **107**, 2357–2362.
3 M. N. R. Ashfold, N. H. Nahler, A. J. Orr-Ewing, O. P. J. Vieuxmaire, R. L. Toomes, T. N. Kitsopoulos, I. A. Garcia, D. A. Chestakov, S.-M. Wu and D. H. Parker, *Phys. Chem. Chem. Phys.*, 2005, **8**, 26–53.
4 A. I. Chichinin, K.-H. Gericke, S. Kauczok and C. Maul, *Int. Rev. Phys. Chem.*, 2009, **28**, 607–680.
5 T. A. Spiglanin, D. W. Chandler and D. H. Parker, *Chem. Phys. Lett.*, 1987, **137**, 414–420.
6 E. d. Beer, B. G. Koenders, M. P. Koopmans and C. A. d. Lange, *J. Chem. Soc., Faraday Trans.*, 1990, **86**, 2035–2041.
7 D. S. Green, G. A. Bickel and S. C. Wallace, *J. Mol. Spectrosc.*, 1991, **150**, 303–353.
8 D. S. Green, G. A. Bickel and S. C. Wallace, *J. Mol. Spectrosc.*, 1991, **150**, 354–387.
9 D. S. Green, G. A. Bickel and S. C. Wallace, *J. Mol. Spectrosc.*, 1991, **150**, 388–469.
10 K. Wang and V. McKoy, *J. Chem. Phys.*, 1991, **95**, 8718–8724.
11 Y. Xie, P. T. A. Reilly, S. Chilukuri and R. J. Gordon, *J. Chem. Phys.*, 1991, **95**, 854–864.
12 D. S. Green and S. C. Wallace, *J. Chem. Phys.*, 1992, **96**, 5857–5877.
13 E. d. Beer, W. J. Buma and C. A. deLange, *J. Chem. Phys.*, 1993, **99**, 3252–3261.
14 Á. Kvaran, H. Wang and Á. Logadóttir, *Recent Res. Devel. in Physical Chem.*, Transworld Research Network, 1998, vol. 2, pp. 233–244.
15 Á. Kvaran, Á. Logadóttir and H. Wang, *J. Chem. Phys.*, 1998, **109**, 5856–5867.
16 H. M. Lambert, P. J. Dagdigian and M. H. Alexander, *J. Chem. Phys.*, 1998, **108**, 4460.
17 P. M. Regan, S. R. Langford, D. Ascenzi, P. A. Cook, A. J. Orr-Ewing and M. N. R. Ashfold, *Phys. Chem. Chem. Phys.*, 1999, **1**, 3247–3251.
18 Á. Kvaran, H. Wang and Á. Logadóttir, *J. Chem. Phys.*, 2000, **112**, 10811–10820.
19 P. M. Regan, D. Ascenzi, A. Brown, G. G. Balint-Kurti and A. J. Orr-Ewing, *J. Chem. Phys.*, 2000, **112**, 10259–10268.
20 Á. Kvaran, H. Wang and B. G. Waage, *Can. J. Phys.*, 2001, **79**, 197–210.
21 H. Wang and Á. Kvaran, *J. Mol. Struct.*, 2001, **563**, 235–239.
22 Á. Kvaran and H. Wang, *Mol. Phys.*, 2002, **100**, 3513–3519.
23 Á. Kvaran and H. Wang, *J. Mol. Spectrosc.*, 2004, **228**, 143–151.
24 Á. Kvaran, H. S. Wang, K. Matthiasson, A. Bodi and E. Jonsson, *J. Chem. Phys.*, 2008, **129**, 164313.
25 K. Matthiasson, H. S. Wang and Á. Kvaran, *J. Mol. Spectrosc.*, 2009, **255**, 1–5.
26 A. Kvaran, K. Matthiasson and H. S. Wang, *J. Chem. Phys.*, 2009, **131**, 044324.
27 K. Matthiasson, J. M. Long, H. S. Wang and Á. Kvaran, *J. Chem. Phys.*, 2011, **134**, 164302.
28 J. Long, H. Wang and Á. Kvaran, *J. Chem. Phys.*, 2013, **138**, 044308.
29 R. Callaghan and R. J. Gordon, *J. Chem. Phys.*, 1990, **93**, 4624–4636.
30 K. Wang and V. McKoy, *J. Chem. Phys.*, 1991, **95**, 7872–7879.
31 D. Ascenzi, S. Langford, M. Ashfold and A. Orr-Ewing, *Phys. Chem. Chem. Phys.*, 2001, **3**, 29–43.
32 J. Long, H. Wang and Á. Kvaran, *J. Mol. Spectrosc.*, 2012, **282**, 20–26.
33 J. Long, H. R. Hrodmarsson, H. Wang and Á. Kvaran, *J. Chem. Phys.*, 2012, **136**, 214315.
34 S. A. Wright and J. D. McDonald, *J. Chem. Phys.*, 1994, **101**, 238–245.
35 S. T. Pratt and M. L. Ginter, *J. Chem. Phys.*, 1995, **102**, 1882–1888.
36 S. R. Langford, P. M. Regan, A. J. Orr-Ewing and M. N. R. Ashfold, *Chem. Phys.*, 1998, **231**, 245–260.
37 P. M. Regan, D. Ascenzi, C. Clementi, M. N. R. Ashfold and A. J. Orr-Ewing, *Chem. Phys. Lett.*, 1999, **315**, 187–193.
38 P. M. Regan, D. Ascenzi, E. Wrede, P. A. Cook, M. N. R. Ashfold and A. J. Orr-Ewing, *Phys. Chem. Chem. Phys.*, 2000, **2**, 5364–5374.
39 H. R. Hrodmarsson, H. S. Wang and Á. Kvaran, *J. Mol. Spectrosc.*, 2013, **290**, 5–12.
40 H. R. Hrodmarsson, H. S. Wang and A. Kvaran, *J. Chem. Phys.*, 2014, **140**, 244304.
41 H. R. Hrodmarsson, H. S. Wang and Á. Kvaran, *J. Chem. Phys.*, 2015, **142**, 244312.
42 H. R. Hrodmarsson and Á. Kvaran, *Phys. Chem. Chem. Phys.*, 2015, **17**, 32517–32527.
43 T. P. Rakitzis, P. C. Samartzis, R. L. Toomes, T. N. Kitsopoulos, A. Brown, G. G. Balint-Kurti, O. S. Vasyutinskii and J. A. Beswick, *Science*, 2003, **300**, 1936–1938.
44 T. P. Rakitzis, P. C. Samartzis, R. L. Toomes, L. Tsigaridas, M. Coriou, D. Chestakov, A. Eppink, D. H. Parker and T. N. Kitsopoulos, *Chem. Phys. Lett.*, 2002, **364**, 115–120.
45 C. Romanescu, S. Manzhos, D. Boldovsky, J. Clarke and H. Loock, *J. Chem. Phys.*, 2004, **120**, 767–777.
46 S. Manzhos, C. Romanescu, H. P. Loock and J. G. Underwood, *J. Chem. Phys.*, 2004, **121**, 11802–11809.
47 C. Romanescu and H. P. Loock, *J. Chem. Phys.*, 2007, **127**, 124304.
48 S. Kauczok, C. Maul, A. I. Chichinin and K. H. Gericke, *J. Chem. Phys.*, 2010, **133**, 10.
49 T. P. Rakitzis, P. C. Samartzis, R. L. Toomes and T. N. Kitsopoulos, *J. Chem. Phys.*, 2004, **121**, 7222–7227.
50 C. Romanescu and H. P. Loock, *Phys. Chem. Chem. Phys.*, 2006, **8**, 2940–2949.
51 D. Zaouris, A. Kartakoullis, P. Glodic, P. C. Samartzis, H. R. Hrodmarsson and A. Kvaran, *Phys. Chem. Chem. Phys.*, 2015, **17**, 10468–10477.
52 P. M. Regan, S. R. Langford, A. J. Orr-Ewing and M. N. R. Ashfold, *J. Chem. Phys.*, 1999, **110**, 281–288.
53 A. G. Smolin, O. S. Vasyutinskii, G. G. Balint-Kurti and A. Brown, *J. Phys. Chem. A*, 2006, **110**, 5371–5378.
54 R. Baumfalk, U. Buck, C. Frischkorn, N. H. Nahler and L. Huwel, *J. Chem. Phys.*, 1999, **111**, 2595.

55 D. A. Chapman, K. Balasubramanian and S. H. Lin, *Chem. Phys.*, 1987, **118**, 333–343.
56 A. Banichevich, R. Klotz and S. D. Peyerimhoff, *Mol. Phys.*, 1992, **75**, 173–188.
57 G. Péoux, M. Monnerville, T. Duhoo and B. Pouilly, *J. Chem. Phys.*, 1997, **107**, 70.
58 B. Pouilly and M. Monnerville, *Chem. Phys.*, 1998, **238**, 437–444.
59 T. P. Rakitzis, P. C. Samartzis, R. L. Toomes, L. Tsigaridas, M. Coriou, D. Chestakov, A. T. J. B. Eppink, D. H. Parker and T. N. Kitsopoulos, *Chem. Phys. Lett.*, 2002, **364**, 115–120.
60 P. M. Regan, S. R. Langford, A. J. Orr-Ewing and M. N. R. Ashfold, *J. Chem. Phys.*, 1999, **110**, 281–288.
61 R. Baumfalk, U. Buck, C. Frischkorn, N. H. Nahler and L. Huwel, *J. Chem. Phys.*, 1999, **111**, 2595.
62 A. I. Chichinin, C. Maul and K.-H. Gericke, *J. Chem. Phys.*, 2006, **124**, 224324.
63 A. I. Chichinin, P. S. Shternin, N. Gödecke, S. Kauczok, C. Maul, O. S. Vasyutinskii and K.-H. Gericke, *J. Chem. Phys.*, 2006, **125**, 034310.
64 P. Glodic, D. Zaouris, P. C. Samartzis, A. Haflidason and Á. Kvaran, *Phys. Chem. Chem. Phys.*, 2016, **18**, 26291–26299.
65 C. R. Gebhardt, T. P. Rakitzis, P. C. Samartzis, V. Ladopoulos and T. N. Kitsopoulos, *Rev. Sci. Instrum.*, 2001, **72**, 3848.
66 V. Papadakis and T. N. Kitsopoulos, *Rev. Sci. Instrum.*, 2006, **77**, 5.
67 P. C. Samartzis, I. Sakellariou, T. Gougousi and T. N. Kitsopoulos, *J. Chem. Phys.*, 1997, **107**, 43–48.
68 See ESI.†.
69 T. Kinugawa and T. Arikawa, *J. Chem. Phys.*, 1992, **96**, 4801–4804.
70 D. S. Ginter, M. L. Ginter and S. G. Tilford, *J. Mol. Spectrosc.*, 1981, **90**, 152–176.
71 G. J. Vázquez, H. P. Liebermann and H. Lefebvre-Brion, (unpublished).